sustainability

MDPI

Article

Brushite-Metakaolin Composite Geopolymer Material as an Effective Adsorbent for Lead Removal from Aqueous Solutions

Dunja Djukić [1], Aleksandar Krstić [2], Ksenija Jakovljević [1], Svetlana Butulija [3], Ljubica Andjelković [4], Vladimir Pavlović [5,*] and Miljana Mirković [3]

[1] Faculty of Biology, University of Belgrade, 11000 Belgrade, Serbia; e3003_2019@stud.bio.bg.ac.rs (D.D.); kjakovljevic@bio.bg.ac.rs (K.J.)
[2] Department of Physical Chemistry, "Vinča" Institute of Nuclear Sciences—National Institute of the Republic of Serbia, University of Belgrade, P.O. Box 522, 11000 Belgrade, Serbia; aleksandar.krstic@vin.bg.ac.rs
[3] Department of Materials, "Vinča" Institute of Nuclear Sciences—National Institute of the Republic of Serbia, University of Belgrade, P.O. Box 522, 11000 Belgrade, Serbia; svetlana8@vin.bg.ac.rs (S.B.); miljanam@vinca.rs (M.M.)
[4] Department of Chemistry, Institute of Chemistry, Technology and Metallurgy, University of Belgrade, 11000 Belgrade, Serbia; ljubica@chem.bg.ac.rs
[5] Faculty of Agriculture, University of Belgrade, 11080 Belgrade, Serbia
* Correspondence: vlaver@agrif.bg.ac.rs

Abstract: Newly designed mesoporous brushite-metakaolin-based geopolymer materials were examined with an idea for using this material as a potential adsorbent for Pb(II) removal from aqueous solutions. As a starting component for geopolymer synthesis, a natural raw kaolinite clay with the addition of 2 wt.%, 4 wt.%, 6 wt.%, 8 wt.%, and 10 wt.% of pure brushite was used. Phase, structural, morphological, and adsorption properties of newly synthesized mesoporous brushite-metakaolin geopolymer materials were examined in detail by the means of XRPD, FTIR, SEM-EDS, BET/BJH, and ICP-OES methods. The ICP-OES results showed that the synthesized material samples with 2 wt.%, 4 wt.%, and 6 wt.% of brushite possess significant adsorption properties and the mechanisms of the adsorption process can be attributed to chemisorption. The most notable result is that brushite-metakaolin-geopolymer with 2 wt.% of brushite have the best efficiency removal, more than 85% of Pb(II).

Keywords: environmentally friendly; alkali-activated materials; high lead removal efficiency; natural adsorbents

Citation: Djukić, D.; Krstić, A.; Jakovljević, K.; Butulija, S.; Andjelković, L.; Pavlović, V.; Mirković, M. Brushite-Metakaolin Composite Geopolymer Material as an Effective Adsorbent for Lead Removal from Aqueous Solutions. *Sustainability* **2022**, *14*, 4003. https://doi.org/10.3390/su14074003

Academic Editor: Ihsanullah Ihsanullah

Received: 24 February 2022
Accepted: 25 March 2022
Published: 28 March 2022

1. Introduction

The need for continuous development and progress, especially in urban areas in the last five decades, leads to a significant ecosystem disruption. Water remediation from toxic metal ions presents one of the biggest challenges for environmental safety since such species are constant components of wastewater, arriving as products of mining, stainless steel, automobile, and metal industries. Among many toxic metals, lead is a serious environmental pollutant, thereby posing a threat to humans, animals, and plants through surface and groundwater contamination. Moreover, it is extremely harmful to human health even at very low exposure levels since it causes osteomalacia, stomach insufficiency, heart failure, and elevated blood pressure [1–3]. Among children, at high levels of exposure, lead affects the brain and nervous system development and leads to serious and irreversible damage. Adsorption presents a preferable technique for lead removal from aqueous solutions, due to the simplicity of the efficient and economical process. Although limited by the low capacity of adsorption, narrow effective pH range of application, and negative effect of coexisting ions on the removal process, many natural and waste materials were

examined as adsorbents of different pollutants [4–7]. Therefore, significant attention has been dedicated to protecting and conserving the environment using newly designed materials with the recycling and reusing mechanism [8]. Clay sediments after leaving open mines remain unused, while the clay itself is of very high quality, just like the clay from the Rudovci site (Lazarevac, Serbia). The potential reuse of this clay is the topic of various authors from this region [9–12]. The main inorganic polymers synthesized from metakaolin have been leading materials in the past two decades, called geopolymer materials [13]. Nowadays, geopolymer materials are increasingly being used as an alternative to cementitious materials due to their strength, fire resistance, rapid curing, low energy, and CO_2 consumption [14]. Moreover, their chemical similarity to zeolites makes them promising adsorbents for the removal of various heavy metals such as Ni(II), Pb(II), Cd(II), and so forth. Therefore, many recent studies have dealt with the possibility of modifying and developing advanced composite geopolymer materials for wastewater treatment [15–17]. The eco-friendly synthesis of modified geopolymer materials often includes mixing natural and abundant starting materials or waste materials with different ratios of materials from the group of calcium-phosphates. A few studies investigated the effects of calcium-phosphate compounds on the metakaolin-based geopolymer composition and structural properties [18,19]. Brushite ($CaHPO_4{\cdot}2H_2O$) belongs to the group of calcium-phosphate materials, and it is characterized by suitable structural, morphological, and adsorption properties. Moreover, it is an environmentally friendly material due to its chemical composition [20,21]. Some phosphate materials such as brushite, monetite, tricalcium phosphate, or hydroxyapatite can be used as starting components of calcium and phosphate ions. Since the pH of the medium affects the solubility of the metal ion, during geopolymerization calcium can replace sodium ions and phosphates can replace some silicates in the metakaolin geopolymer structure. This leads to the formation of semi-crystalline geopolymer material, where structural changes do not affect the neutrality of the system [22]. We assume that metakaolin geopolymer structure can be improved in the meaning of adsorption characteristics by adding pure brushite material during synthesis, for obtaining mesoporous material. In the spirit of green chemistry, environmental protection, and reuse of abandoned clay deposits, we used metakaolin with the addition of brushite material, merging them into new brushite-metakaolin-geopolymer material (GPB). The need for such research is reflected in the fact that residual, natural materials would be used to purify water from heavy metals. This process is otherwise very expensive and complicated, and the newly synthesized materials, in addition to being inexpensive, could be reused after the desorption of heavy metals [23–25]. This also reduces waste accumulation and affects the recovery of residual clay sediments and environmental pollution. Moreover, the synthesis process of brushite we performed in this research is simple, inexpensive, and the by-products are not harmful to the environment [21]. Extensive anthropogenic activities such as mining, agricultural processes, and disposal of industrial waste materials are the main sources of increased heavy metal ions concentrations in water [26]. Therefore, we consider the need to design new mesoporous geopolymeric materials obtained from raw and eco-friendly materials as adsorbents for lead.

The main idea of this research was to synthesize mesoporous brushite-metakaolin geopolymer materials with good adsorbent properties for lead ions removal from water. Due to their good hydrophilic properties and mesoporosity, obtained brushite-metakaolin geopolymer-based materials were thoroughly examined in the present study.

2. Materials and Methods

2.1. Materials

Brushite was synthesized by the solution-precipitation reaction, previously described by Mirković et al. [21]. The kaolinite clay used in this experiment is high-quality kaolinite clay, from abandoned deposit Rudovci, Lazarevac district (Serbia). Physico-

chemical characteristics of kaolinite are previously described by Nenadović et al. [9]. Kaolinite was thermally treated at 750 °C for one hour to produce metakaolin and to release residual impurities and organic matter. The activator solution was prepared from sodium-silicate and 6M NaOH solution (analytical grade) in relation to 1:1.6. In metakaolin, 2 wt.%, 4 wt.%, 6 wt.%, 8 wt.%, and 10 wt.% of pure brushite material was added, followed by the activation reaction–activator solution was added in order to induce polymerization reaction. The obtained GPB material was put into conic molds and left to age for 28 days at room temperature.

For phase analysis of synthesized materials, the method of x-ray diffraction (XRD) analysis was used. Powdered samples were characterized at room temperature using an Ultima IV Rigaku diffractometer, equipped with CuK$\alpha_{1,2}$ radiations, using a generator voltage (40.0 kV) and a generator current (40.0 mA). The range of 5–60° 2θ was used for all powders in a continuous scan mode with a scanning step size of 0.02° and at a scan rate of 10 °/min using D/TeX Ultra high-speed detector. A high-purity single-crystal silicon sample carrier was used, where samples are placed. The samples are previously prepared to a grain size of fine powder in a porcelain mortar. The PDXL2 (Ver. 2.8.4.0) software was used to evaluate the phase composition and identification [27]. All obtained powders were identified using the ICDD database [28]. Selected ICDD card numbers used for identifications were: brushite: 01-072-0713, quartz: 01-075-8322, muscovite: 01-074-6686, and albite: 01-089-6427.

Diffuse reflectance infrared Fourier transform spectroscopy (DRIFT) was used for functional groups study of GPB samples. Spectra were taken at room temperature using a Thermo Scientific Nicolet iS10, FT-IR Spectrometer in a working range 4000–450 cm^{-1}. The samples were prepared by dispersing approximately 5% of the sample in dried KBr (spectroscopic grade) with a refractive index of 1.559 and particle size 5–20 μm, and the diffuse reflectance spectra were obtained.

Morphological properties of materials and semi-quantitative elemental analysis were performed using SEM-EDS analysis. All samples were Au-coated and examined using the JEOL JSM 6390 LV electron microscope at 30 kV.

The specific surface area (S_{BET}) and the pore size distribution (PSD) of samples GPB 2%, GBP 4%, and GBP 6% were analyzed using the Surfer (Thermo Fisher Scientific, Waltham USA). Prior to analyses, the samples were degassed at 105 °C for 4 h under vacuum. By applying the BJH method, pore size distribution (PSD) was estimated [29] to the desorption branch of isotherms, while mesopore surface and micropore volume were calculated using the *t*-plot method [30].

2.2. Adsorption Studies

The preliminary adsorption experiments revealed that the removal efficiency of Pb (II) for GPB 2% sample was 87%. The brushite addition in metakaolin hybrid geopolymer samples led to the decreases of Pb (II) removal efficiency to 78% for GBP 4% and 62% for GPB 6%. Lead removal efficiency was lower than 50% for GPB 8% and GPB 10% samples. Therefore, GPB 8% and GPB 10% were excluded from further study.

Thermo Scientific Orion Star A221 pH portable meter was used to determine pH values in all prepared solutions. The pH values of the point of zero charge (pH_{PZC}) of GPB 2%, GPB 4%, and GPB 6% were determined by the pH drift method (10.1016/j.watres.2004.01.034, accessed on 1 November 2021). Sodium chloride solutions (0.01 M, 25 mL) were prepared in the closed Erlenmeyer flasks. Sodium hydroxide (0.1 M) and hydrochloric acid (0.1 M) solutions were used for pH adjustment between 2 and 12. In each prepared solution 75 mg of GPB 2%, GPB 4% and GPB 6%, were added. The final pH values were determined after 48 h at room temperature. The pH_{pzc} values were found at the point where the curve pH_{final} vs. pH_{inital} crosses the line $pH_{initial} = pH_{final}$. In order to investigate the applicability of all GPB samples as adsorbents of Pb(II), a batch adsorption studies were performed. Analytical grade $Pb(CH_3COO)_2$ was used to prepare the Pb(II)

stock solutions. All GPB samples were contaminated with obtained solutions at the temperature of 25 °C. The influence of different parameters, such as solution pH (4–10), contact time (10–1440 min), and initial metal ion concentration (10–200 mg/L) was investigated. A few drops of 0.5 M HNO_3 or NaOH were added to the lead acetate solution in order to adjust the pH values. After the pH adjustments, 20 mL of lead acetate solution ($C_{(Pb)}$ = 10 mg L^{-1}) was shaken with 50 mg of each GPB sample on orbital shaker model Stuart SSL 1 at a speed rate 170 rpm for three hours. Furthermore, the dependence of the lead adsorption on the GPB 2%, GBP 4%, and GBP 6% samples for different contact time (pH = 5.5, $C_{(Pb)}$ = 10 mg L^{-1}, $m_{(GPBs)}$ = 50 mg, V = 20 mL, 25 °C) and initial metal ion concentration (pH = 5.5, $m_{(GPBs)}$= 50 mg, $t_{(GPB\ 2\%)}$ = 300 min, $t_{(GPB\ 4\%)}$ = 120 min, $t_{(GPB\ 6\%)}$ = 120 min, V = 20 mL, 25 °C) were investigated. The residual concentrations of lead ions were determined by ICP-OES spectrometer (Thermo Fisher Scientific ICAP 7400 duo) in triplicate. The lead was analyzed on 220.353 nm wavelength.

Besides obtaining pH values of the pH_{PZC}, in order to determine the adsorption mechanism, adsorption isotherms and kinetic models were used, to confirm the results.

The quantities that characterize the adsorption process are the adsorption capacity and the adsorption efficiency. The amount of lead that is adsorbed per unit mass of adsorbent until equilibrium is established, q_e (mg/g), depending on parameters and is defined by Equation (1):

$$q_e = \frac{(C_0 - C_e)V}{m} \quad (1)$$

where c_0 is the initial concentration of a lead solution (mg dm^{-3}), *Ce* is a concentration of lead solution after equilibrium concentration (mg dm^{-3}), *m* is the mass of adsorbent-GPB (g), *V* is the volume of lead solution (dm^3).

The adsorption efficiency *R* (%) is defined by the following Equation (2):

$$(\%)\ removal\ = \frac{C_0 - C_e}{C_0}\ \times 100 \quad (2)$$

3. Results and Discussion

3.1. XRD Results

Phase results of XRD analysis of synthesized GPB materials are shown in Figure 1.

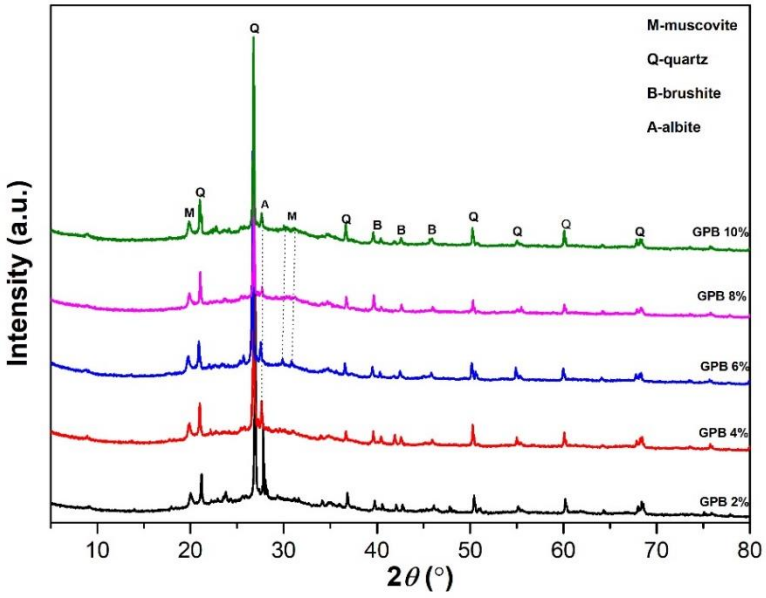

Figure 1. XRD of GPB materials.

Quartz is the major secondary mineral that occurs with clay minerals [31]. It is clear that during the geopolymerization process, primary structures are disturbed and show high background which is characteristic for the amorphous matrix due to the geopolymerization process in the range between 20–40 °2θ. In this case, the observed powder diffractogram indicated the semi-crystalline structural arrangement of GPB materials. The sharp undisturbed peaks of quartz are evident in all five samples since the crystal grains of quartz remain unchanged in the matrix during the process of alkaline activation. The main difference between GPB 2% sample and other samples is a sharp and narrow peak at about 27 °2θ, belonging to sodium tecto-alumotrisilicate, i.e., albite with corresponding chemical composition $NaAlSi_3O_8$. This can be explained by the fact that the highest amount of activator solution is added in relation to the added brushite powder. The intensity of the albite peak is decreasing equally in other samples according to diffraction results. This phenomenon can be described by the contribution of Na, Al, and Si in the geopolymer matrix from alkali activator solution and possible preferential orientation of albite. We assume that, while during the geopolymerization process in other samples, there is a greater consumption of these elements from the alkaline activator, which indicates a reduction in peaks and its lower intensities. The albite is very often altered by different thermodynamic processes in nature; it also has a low arrangement of the structural lattice, and possibly its upgrade in the first sample can be partly explained by the partial structural ordering of low-order triclinic albite in a geopolymer matrix by 28 days aging process. It is evident that peaks belonging to the brushite phase decreased by increasing its concentration in a geopolymer matrix, as a sign of incorporation of brushite in the amorphous matrix due to the geopolymerization process.

3.2. DRIFT Analysis Results

The results of DRIFT, presented in Figure 2, are used to determine and explain the functional groups of synthesized GPB samples.

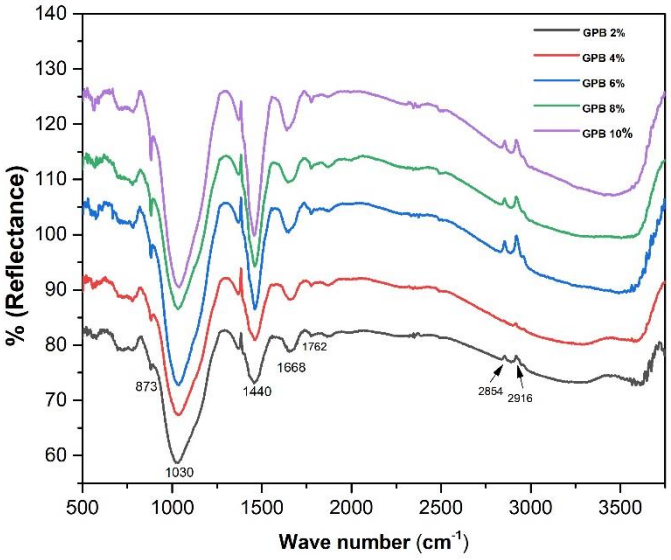

Figure 2. DRIFT spectra of synthesized GPB samples.

The two bands near 3500 and 1670 cm^{-1} are related to the presence of free or adsorbed water in all samples. This indicates that material contains sialon group and residual structural water, which is very common in clays [18].

The band that appears at about 560 cm^{-1} is characteristic for brushite-metakaolin types of cement and could be ascribed to –P–O–Al–O– molecule polymer vibration. [18]. The band at about 712 cm^{-1} belongs to Si-O-Al bending vibration and points that the main

geopolymer structure, after the brushite addition and after the reaction of silicon and aluminates, was Si-O-Al. The band at 873 cm^{-1} is attributed to Si-O-Si vibrations. The wide stretched band at about 1030 cm^{-1} can be related to inclusions of PO_4 tetrahedral units in geopolymer cement system to form an –Si–O–Si–O–Al–O–Si–O–P–O– network. Additionally, the presence of Ca from the brushite structure could densify and balance the charge in the system. Published studies so far, in the case of the addition of 4%, 6%, 8%, and 10% of brushite, were suggesting the modifications of the network due to the incorporation of phosphorous groups [18,32]. The band that appears at about 1440 cm^{-1} belongs to the formation of the non-centric carbonate group and Na^+ from alkaline solution attached to CO_2 from the air. The intensity of these bands is higher in the IR spectra of GPB 10%, GPB 8%, and GPB 6%. This higher intensity could be related to the higher amount of Ca in the system, which attracts CO_2 from the atmosphere [18].

3.3. SEM-EDS Analysis Results

Figure 3 represents SEM images of investigated GPB materials. Brushite in all samples is characterized by plate-like highly crystalline grains, with proper monoclinic forms. The measured grains have sizes between 1.04 μm and 2.40 μm. Obviously, the matrix of samples consisted of clay flakes since clay is an agglomerate of various fine-grained minerals. Agglomerates consisted of fine-grained particles that vary in size from 928 nm to 274 nm, approximately. The quartz phase confirmed by XRPD is most likely located in the interspaces between interconnected particles. The SEM micrographs of synthesized GPB materials revealed the presence of spherical agglomerative forms, indicating that the geopolymerization process occurred. Such a process led to the structural collapsing and formation of amorphous geopolymer, corroborating XRPD results. The grains that formed the geopolymer matrix were finely glued together into a single geopolymer mass. Besides, there were unaltered mineral grains, confirming semi-crystalline structures. It is obvious that GPB 2% sample (Figure 3) revealed morphology such that the grains of brushite are preserved. The presence of a clearly visible geopolymer matrix around them is confirmed, as shown in Figure 3. In this case, brushite is not completely dissolved in the matrix which is deduced previously by XRPD analysis. As can be seen in Figure 3, the surface of GPB 4% and GPB 6% materials consisted of brushite grains covered to a greater extent with an amorphous geopolymer matrix. The higher the weight concentration of brushite is, the greater interconnection of matrix particles occurs. Micrograph of GPB 8% revealed localization of lamellar interconnected brushite grains. The GPB material with the highest brushite concentration is shown in Figure 3 (GPB 10%). In this case, completely homogeneous texture is obtained.

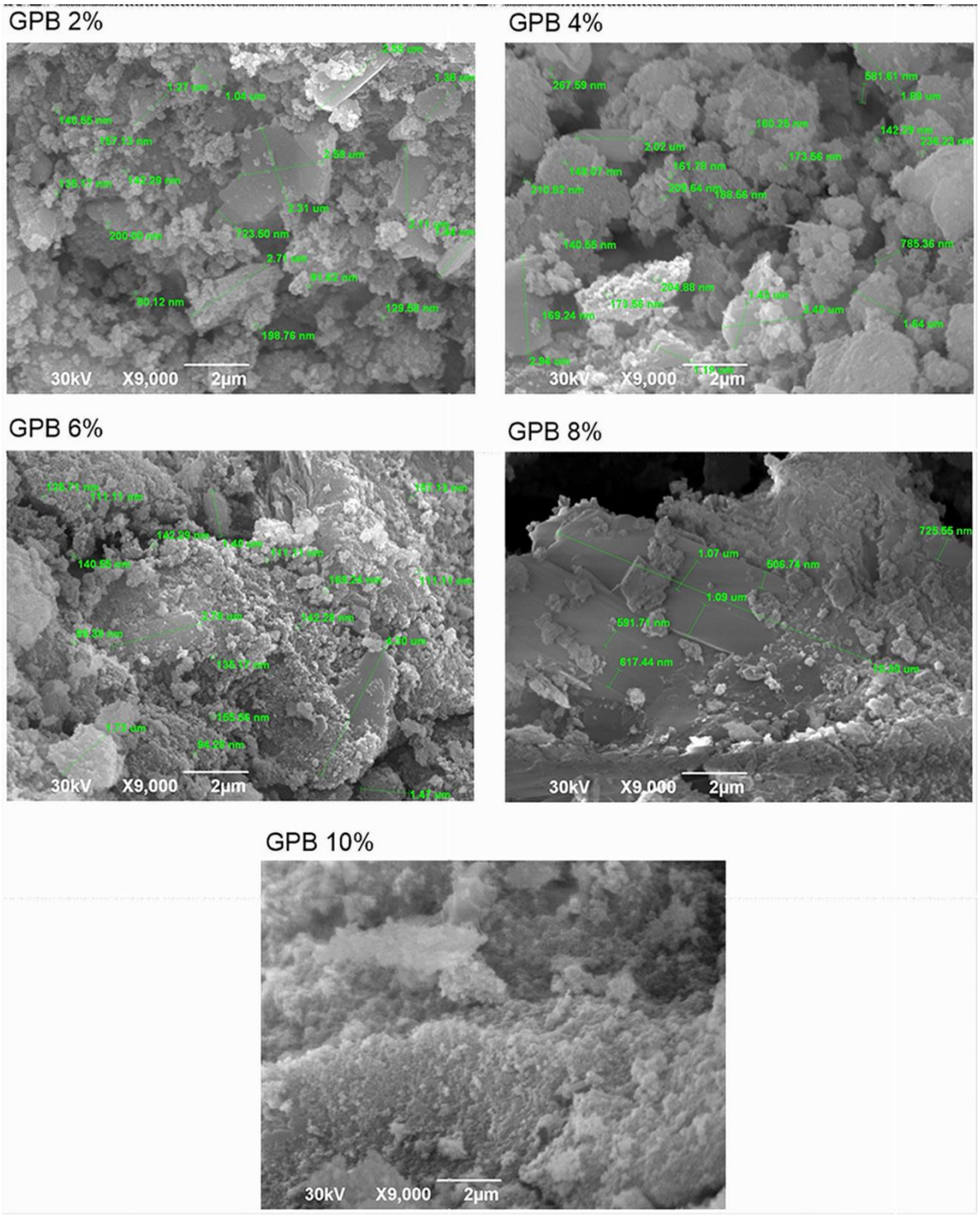

Figure 3. SEM micrographs of synthesized GPB samples.

The EDS results of obtained materials are presented in Table 1. Based on the EDS results, the content of Ca and P increases properly with the added content of brushes in the geopolymer matrix. Based on EDS semi quantitative analysis calculated ratio Si:Al:Na is near 2:1:1.

Table 1. EDS results for the synthesized samples.

Element wt (%)	GPB 2%	GPB 4%	GPB 6%	GPB 8%	GPB 10%
Na	27.62	27.02	27.44	26.94	27.62
Al	26.67	26.52	26.48	26.08	26.02
Si	42.71	42.68	42.86	41.94	41.83
P	0.64	0.72	0.79	0.96	0.99
K	0.67	0.45	0.48	0.86	0.57
Ca	0.86	0.93	1.02	1.72	1.90
Fe	0.83	1.68	0.93	1.50	1.07
Total	100.00	100.00	100.00	100.00	100.00

3.4. BET Analysis Results

Nitrogen adsorption isotherms for GPB samples, as the amount of N_2 adsorbed at −196 °C, are shown in Figure 4. According to the IUPAC classification [33], isotherms are of type-IV and with an H3 hysteresis loop which is associated with mesoporous materials. The specific surface area of all samples, calculated by the BET equation, lies between 20 and 27 m^2/g, and the median pore radius, r_{med} is ~11 nm for all three samples.

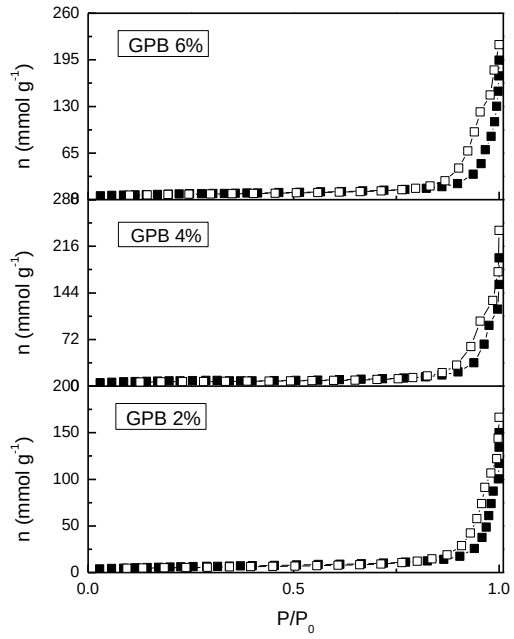

Figure 4. Nitrogen adsorption isotherm plot for GPB samples. Solid symbols–adsorption, open symbols–desorption.

Pore size distribution (PSD) of GPB samples is presented in Figure 5. It can be seen that for all the samples, the pore radius lies between 4 and 45 nm, indicating that all three samples are completely mesoporous (according to IUPAC classification: micropores ≤ 2 nm, mesopores 2–50 nm, and macropores ≥ 50 nm), as a consequence of the particles' agglomeration.

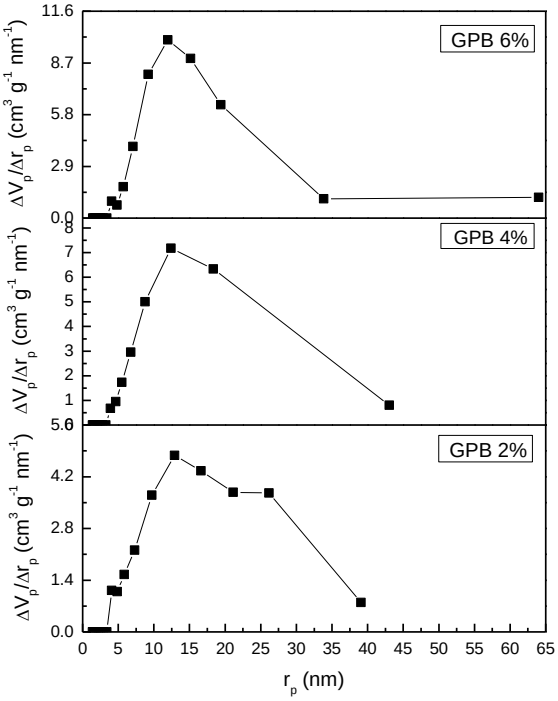

Figure 5. Pore size distribution of GPB samples.

3.5. Adsorption Studies

3.5.1. Effect of pH

The pH_{PZC} is a measure of the adsorbent's acidity/basicity and its net surface charge [34]. The determined pH_{PZC} values of all investigated samples are about 10.7, Figure 6.

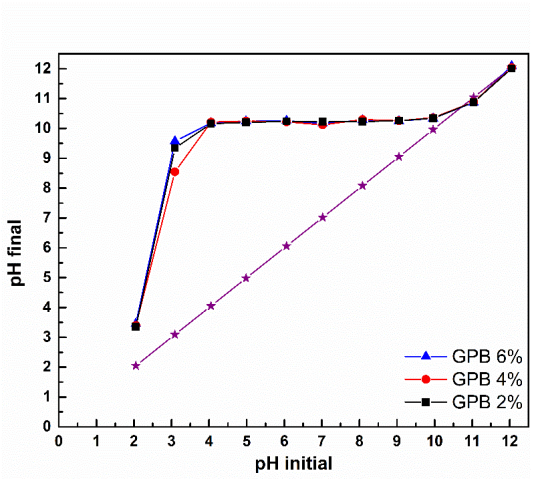

Figure 6. The pH_{PZC} values for GPB 2%, GPB 4%, and GPB 6% samples.

The effect of pH on the Pb(II) sorption onto GPB 2%, GPB 4%, and GPB 6% is shown in Figure 7. The pH values under 4.0 were not taken into consideration since Ca^{2+} release from the GPB structure can be significant in such conditions. The removal efficiency is the highest for the pH values above 7.0 for all investigated GPBs. However, in alkaline conditions, Pb(II) hydrolysis occurs due to the formation of lead hydroxide precipitation. Therefore, such results cannot be taken into consideration. The slightly acidic conditions are

proven to be optimal for such systems, especially for GPB 2%, as shown in Figure 7. Considering these facts, and considering that wastewaters rich in lead species are acidic, all further adsorption experiments were performed at the pH value 5.5.

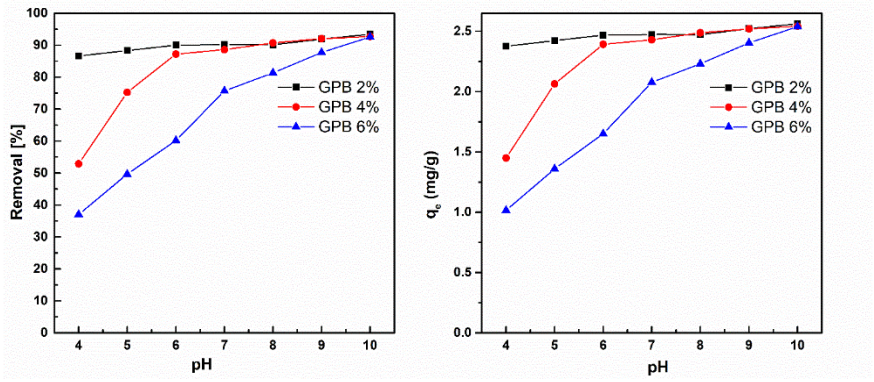

Figure 7. Pb(II) removal percentages (**left**) and adsorption capacities (**right**) as a function of pH (contact time = 180 min, $C_{Pb(II)}$ = 6.86 mg/L, V = 20 mL, $m_{adsorbent}$ = 50 mg).

3.5.2. Adsorption Studies—Effect of Contact Time and Kinetic Study

The efficiency of Pb(II) removal as a function of contact time is shown in Figure 8a. The adsorption equilibrium was achieved in 120 min for all investigated GPBs. It should be emphasized that GPB 2% sorbents removed about 85% of Pb(II) (Figure 8a). After 120 min, changes in Pb(II) removal were negligible due to the saturation of the available binding sites. There is no significant change in adsorption capacity after 120 min.

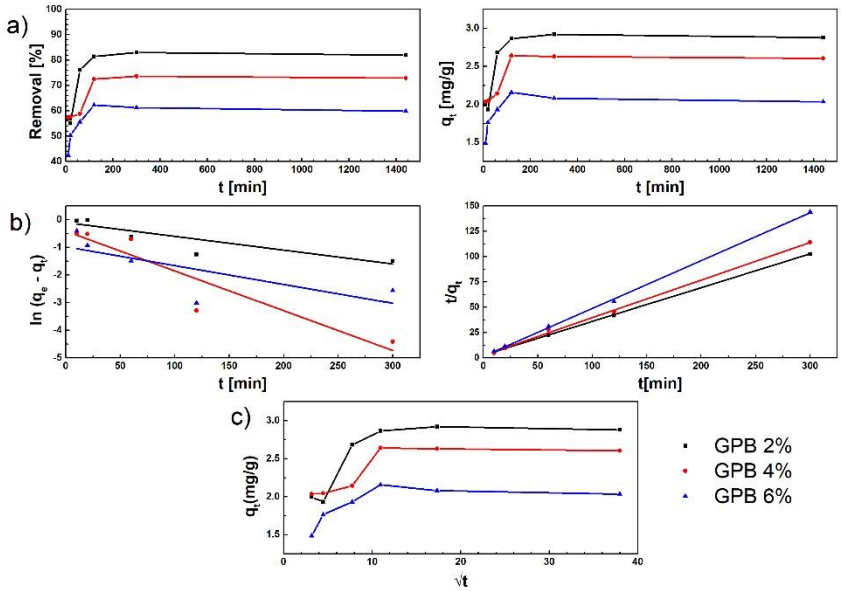

Figure 8. (**a**) Pb(II) removal percentages (left) and adsorption capacities (right) as a function of contact time; (**b**) linearized forms of pseudo-first and pseudo-second kinetic order models (**c**) intraparticle diffusion model (pH = 5.5, $C_{Pb(II)}$ = 8.8 mg/L, V = 20 mL, $m_{adsorbent}$ = 50 mg).

To gain deeper insight into the mechanism of adsorption and kinetic parameters, pseudo-first and pseudo-second kinetic models have been used to verify the experimental data (Figure 8b). The linearized forms of these models are given in Equations 3 and 4, respectively:

$$ln(q_e - q_t) = lnq_e - \frac{k_1}{2.303}\, t \quad (3)$$

$$\frac{t}{q_t} = \frac{1}{k_2 q_e^2} + \frac{t}{q_e} \quad (4)$$

where

t is adsorption process time (min),

q_t is adsorption capacity of the GPB adsorbents, (mg g^{-1}),

q_e is adsorption capacity of the adsorbent at equilibrium (mg g^{-1}),

k_1 is the pseudo-first order model's adsorption rate constant (min^{-1}), and

k_2 is the pseudo-second order model's adsorption rate constant [g (mg min)$^{-1}$].

Parameters obtained from kinetic models are given in Table 2. Pseudo-second order ($R^2 \approx 1$, $q_{e\,(cal)} \approx q_{e\,(exp)}$) fits much better than pseudo-first order (Table 2, Figure 8b), indicating that the chemisorption is the dominant adsorption mechanism [35].

Table 2. Adsorption kinetics models parameters.

Sample	Model	Parameter	Value
GBP2%	Pseudo-first order	k_1	−0.0050
		q_e	0.9014
		R^2	0.8660
	Pseudo-second order	k_2	0.0428
		q_e	2.9949
		R^2	1.0000
GBP4%	Pseudo-first order	k_1	−0.0144
		q_e	1.5083
		R^2	0.8250
	Pseudo-second order	k_2	0.0542
		q_e	2.6923
		R^2	0.9997
GBP6%	Pseudo-first order	k_1	−0.0068
		q_e	0.3755
		R^2	0.3976
	Pseudo-second order	k_2	0.1422
		q_e	2.1169
		R^2	0.9999

In spite of the fact that the pseudo-second order kinetic model can appropriately describe adsorption kinetic experimental data, this model cannot fully explain adsorption mechanism [36]. Pseudo-first and pseudo-second models do not take diffusion into account. However, intra-particle diffusion may affect kinetic measurements. Therefore, the intra-particle diffusion model was used to identify the reaction pathways and adsorption mechanisms. The linearized transformation of this model is presented in Equation 5

$$q_t = kp \cdot t^{1/2} + C \quad (5)$$

where

kp is the rate constant of the intra-particle diffusion model (mg g^{-1} x $min^{1/2}$) and

C is a constant associated with thickness of the boundary layer (mg g^{-1}).

The q_t versus $t^{1/2}$ plots are shown in Figure 8c. Intra-particle diffusion presents rate-limiting step in the adsorption process if a q_t as a function of $t^{1/2}$ yields a straight line. Since the plots do not pass through the origin, Figure 8c, the intra-particle diffusion alone is not the rate-limiting step [37]. As can be seen from Figure 8c, the adsorption process followed two distinct steps. The first region, recognized by high slope, represents boundary layer

diffusion, while the second one followed intra-particle diffusion. This indicates that the film diffusion also took part in both observed processes [38].

3.5.3. Adsorption Isotherms

The plots of q_e versus C_e for the complete adsorption isotherms are presented in Figure 9. The Langmuir and Freundlich isotherm models were investigated to describe the adsorption equilibrium data. The Langmuir isotherm describes monolayer adsorption onto the homogeneous surface of an adsorbent [39]. The linearized form of Langmuir isotherm is given by Equation 6:

$$\frac{1}{q_e} = \frac{1}{q_m} + \left(\frac{1}{q_m K_l}\right)\frac{1}{C_e} \quad (6)$$

The Freundlich isotherm describes multilayer adsorption on an adsorbent whose surface is heterogeneous. The linear form of Freundlich isotherm can be written as the following Equation:

$$\ln q_e = \ln K_f + 1/n \ \ln C_e \quad (7)$$

q_e is adsorption capacity at equilibrium (mg g^{-1});
q_m is the maximum adsorption capacity (mg g^{-1});
c_e is concentration of lead solution after equilibrium concentration (mg dm^{-3});
K_l is Langmuir isotherm constant ($dm^3\,mg^{-1}$);
K_f is Freundlich isotherm constant (L mg^{-1});
$1/n$ is heterogeneity factor and related to surface heterogeneity;
α_l is a parameter related to adsorption energy and is obtained from the linearly "fitted" graph.
K_l/α_l represents theoretical monolayer saturation capacity. Adsorption is favorable if $1/n$ is smaller than 1 and bigger than 0 [40].

The isotherm parameters of Pb(II) sorption are shown in Table 3. It can be seen from the R^2 values that Freundlich isotherm better describes the adsorption process (Figure 9c). In all cases $1/n$ is between 0 and 1. This confirms that chemisorption process occurred [41].

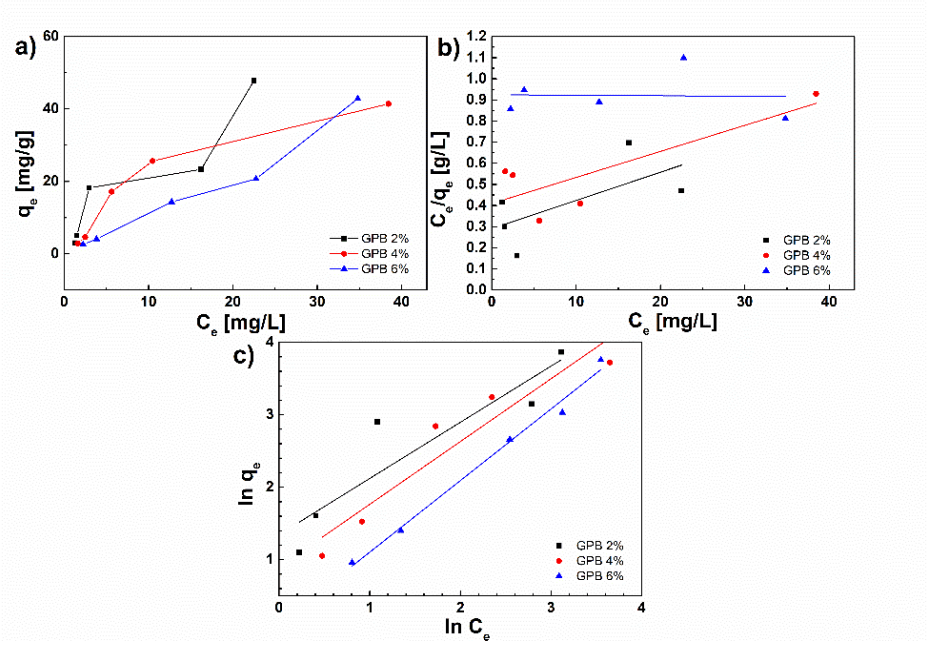

Figure 9. (**a**) The q_e versus *Ce* adsorption isotherm plots for GPB 2%, GPB 4%, and GPB 6%; (**b**) Linearized forms of Langmuir and (**c**) Freundlich isotherm models for Pb(II) adsorption (contact time = 120 min, $C_{Pb(II)}$ = 8.8, 13.9, 48.5, 74.6, 142.1 mg/L, V = 20 mL, $m_{adsorbent}$ = 50 mg, pH = 5.5).

In Table 3, the adsorption isotherm models parameters are given.

Table 3. Adsorption isotherm models parameters.

Sample	Model	Parameter	Value
GBP2%	Langmuir	K_L	3.4447
		α_L	0.0462
		q_m	74.627
		R^2	0.4340
	Freundlich	K_F	3.8359
		$1/n$	0.7757
		R^2	0.8405
GBP4%	Langmuir	K_L	2.4402
		α_L	0.0300
		q_m	81.301
		R^2	0.6716
	Freundlich	K_F	2.4493
		$1/n$	0.8670
		R^2	0.9033
GBP6%	Langmuir	K_L	1.0814
		α_L	−0.0002
		R^2	0.0009
	Freundlich	K_F	1.1196
		$1/n$	0.9889
		R^2	0.9901

Briefly, the results for Pb(II) adsorption directly show that the synthesized GPBs were efficient in the aspect of the necessary time for equilibrium achievement (120 min for all investigated samples). Kinetic studies and adsorption isotherms revealed that the mechanism of Pb(II) removal can be explained as chemisorption. The values of obtained pH_{PZC} were above 10, and the S_{BET} values were quite small. This unambiguously implies that electrostatic interactions and physisorption as the mechanisms of the adsorption process can be excluded. Furthermore, XRD patterns for the samples obtained after the lead adsorption showed that there were no significant changes in the structural properties of the investigated geopolymer materials. Although new phases were not identified, a slightly higher noise of the peaks was observed, indicating that lead ions probably incorporated in the amorphous geopolymer matrix (Figure S1, Supplementary Material). The FT-IR results obtained for GPB materials after the lead adsorption process implied that lead ions formed insoluble lead-carbonate (Figure S2, Supplementary Material). Furthermore, the inclusion of lead into the system led to the slight change of the FT-IR band, which belongs to the vibrations of PO_4 tetrahedral units in geopolymer, as shown in Figures 2 and S2. This corroborates the assumption that lead ions probably incorporated in the amorphous geopolymer matrix. However, there are still many preserved functional groups in the GPB after the adsorption process.

Comparison of the adsorption results with data presented in the literature (Table 4) highlighted that the synthesized GPBs were efficient in the aspect of the necessary time for equilibrium achievement. Having in mind that the removal is directly influenced by initial Pb(II) dosage and adsorbent's concentration, the observed removal percentage in the case of GPB 2% (~85%, $C_{Pb(II)}$ = 142.1 mg/L) is significant. Compared adsorption efficiencies (mg g^{-1} min^{-1}) unambiguously point out that the adsorbents investigated in this work possess remarkable advantages, as shown in Table 4.

Table 4. Adsorption efficiency of different investigated materials.

$C_{oPb(II)}$ (mg/L)	Adsorbent Dosage (mg)	Adsorbent	Removal (%)	Saturation Time (min)	Adsorption Efficiency * (mg g^{-1} min^{-1})	Ref.
400	30	nano-TCP	37.5	60	0.08	[42]
20	10	nano-HAp	99.8	15	0.13	[43]
50	500	MK	98	60	0.002	[12]
50	120	MK-GP	99	60	0.007	[12]
1000	100	FA 35%/MK 65%	65.44	240	0.027	[44]
142.1	50	GPB 2%	84.18	120	0.020	This work
142.1	50	GPB 4%	72.95	120	0.017	This work
142.1	50	GPB 6%	75.52	120	0.018	This work

* Adsorption efficiency = ($C_{oPb(II)}$ · Removal (%))/100% (Adsorbent dosage Saturation time).

4. Conclusions

In this study, mesoporous, natural, and eco-friendly brushite-metakaolin-geopolymer materials were synthesized by the utilization of raw kaolinite and brushite prepared by the Green Chemistry procedure. XRPD results showed the fracture of the high structural order of starting clay materials by the addition of the brushite phase, confirming the incorporation of brushite into the amorphous matrix due to the geopolymerization process. The synthesized GPB materials were investigated as potential adsorbents for Pb(II) removal from aqueous solutions. Prepared GPB 2%, GPB 4%, and GPB 6% showed excellent Pb(II) adsorption properties. For all investigated adsorbents, the equilibrium time was 120 min. In all cases, the adsorption process was described by the Freundlich isotherm model and pseudo-second order model kinetics, indicating that the main adsorption mechanism is chemisorption, corroborating the BET/BJH and pHPZC results. Finally, based on the significant adsorption properties of such materials, as well as the availability of starting components, and low-cost synthesis with reduced energy consumption, it can be concluded that brushite-metakaolin-geopolymer materials could be successfully used for the removal of lead from wastewater.

Supplementary Materials: The following supporting information can be downloaded at: https://www.mdpi.com/article/10.3390/su14074003/s1, Figure S1: XRD results of GPB samples after lead adsorption experiments, Figure S2: DRIFT spectra of GPB materials after lead adsorption experiments.

Author Contributions: Data curation, V.P. and S.B.; Formal analysis, V.P. and A.K.; Investigation, D.D.; Methodology, M.M. and D.D.; Resources, M.M.; Supervision, V.P., M.M., and K.J.; Validation, K.J. and L.A.; Writing—original draft, D.D.; Writing—review & editing, M.M. and L.A.. All authors have read and agreed to the published version of the manuscript. The authors declare that they have no known competing financial interests or personal relationships that could have appeared to influence the work reported in this paper.

Funding: This research was funded by Ministry of Education, Science and Technological Development of Republic of Serbia grant numbers: 451-03-68/2022-14/200017, 451-03-68/2022-14/200026 and 451-03-68/2022-14/200116.

Institutional Review Board Statement: Not applicable.

Informed Consent Statement: Not applicable.

Data Availability Statement: Not applicable.

Conflicts of Interest: The authors declare no conflict of interest.

References

1. Melila, M.; Rajaram, R.; Ganeshkumar, A.; Kpemissi, M.; Pakoussi, T.; Agbere, S.; Lazar, I.M.; Lazar, G.; Amouzou, K.S.; Paray, B.A.; et al. Assessment of renal and hepatic dysfunction by co-exposure to toxic metals (Cd, Pb) and fluoride in people living nearby an industrial zone. *J. Trace Elem. Med. Biol.* **2021**, *69*, 126890. https://doi.org/10.1016/j.jtemb.2021.126890.
2. Gundacker, C.; Forsthuber, M.; Szigeti, T.; Kakucs, R.; Mustieles, V.; Fernandez, M.F.; Bengtsen, E.; Vogel, U.; Hougaard, K.S.; Saber, A.T. Lead (Pb) and neurodevelopment: A review on exposure and biomarkers of effect (BDNF, HDL) and susceptibility. *Int. J. Hyg. Environ. Health* **2021**, *238*, 113855. https://doi.org/10.1016/j.ijheh.2021.113855.
3. Guan, S.; Tao, S.; Huang, Y.; Jin, Y.; Hu, Y.; Lu, J. Combined toxic effects of CBNPs and Pb on rat alveolar macrophage apoptosis and autophagy flux. *Ecotoxicol. Environ. Saf.* **2020**, *205*, 111062. https://doi.org/10.1016/j.ecoenv.2020.111062.
4. Rakhym, A.B.; Seilkhanova, G.A.; Kurmanbayeva, T.S. Adsorption of lead (II) ions from water solutions with natural zeolite and chamotte clay. *Mater. Today Proc.* **2020**, *31*, 482–485. https://doi.org/10.1016/j.matpr.2020.05.672.
5. Chen, P.; Zhai, J.; Sun, W.; Hu, Y.; Yin, Z.; Lai, X. Adsorption mechanism of lead ions at ilmenite/water interface and its influence on ilmenite flotability. *J. Ind. Eng. Chem.* **2017**, *53*, 285–293. https://doi.org/10.1016/j.jiec.2017.04.037.
6. Huda, B.N.; Wahyuni, E.T.; Mudasir, M. Eco-friendly immobilization of dithizone on coal bottom ash for the adsorption of lead(II) ion from water. *Results Eng.* **2021**, *10*, 100221. https://doi.org/10.1016/j.rineng.2021.100221.
7. Fan, L.; Luo, C.; Sun, M.; Li, X.; Qiu, H. Highly selective adsorption of lead ions by water-dispersible magnetic chitosan/graphene oxide composites. *Colloids Surf. B Biointerfaces* **2013**, *103*, 523–529. https://doi.org/10.1016/j.colsurfb.2012.11.006.
8. Perná, I.; Šupová, M.; Hanzlíček, T.; Špaldoňová, A. The synthesis and characterization of geopolymers based on metakaolin and high LOI straw ash. *Constr. Build. Mater.* **2019**, *228*, 116765. https://doi.org/10.1016/j.conbuildmat.2019.116765.
9. Nenadović, S.S.; Kljajević, L.M.; Nešić, M.A.; Petković, M.Ž.; Trivunac, K.V.; Pavlović, V.B. Structure analysis of geopolymers synthesized from clay originated from Serbia. *Environ. Earth Sci.* **2017**, *76*, 1–10. https://doi.org/10.1007/s12665-016-6360-4.
10. Ivanović Marija, K.L.; Jelena, G.; Marijana, P.; Ivona, Ja.; Dušan, B.; Snežana, N. The Effect of the Concentration of Alkaline Activator and Aging Time on the Structure of Metakaolin Based Geopolymer. *Sci. Sinter.* **2020**, *52*, 219–229. https://doi.org/10.2298/SOS2002219I.
11. Mladenović, N.; Kljajević, L.; Nenadović, S.; Ivanović, M.; Čalija, B.; Gulicovski, J.; Trivunac, K. The Applications of New Inorganic Polymer for Adsorption Cadmium from Waste Water. *J. Inorg. Organomet. Polym. Mater.* **2020**, *30*, 554–563. https://doi.org/10.1007/s10904-019-01215-y.
12. Trivunac, K.; Kljajević, L.; Nenadović, S.; Gulicovski, J.; Mirković, M.; Babić, B.; Stevanović, S. Microstructural characterization and adsorption properties of alkali-activated materials based on metakaolin. *Sci. Sinter.* **2016**, *48*, 209–220. https://doi.org/10.2298/SOS1602209T.
13. Si, R.; Dai, Q.; Guo, S.; Wang, J. Mechanical Property, Nanopore Structure and Drying Shrinkage of Metakaolin-based Geopolymer with waste glass powder. *J. Clean. Prod.* **2019**, *242*, 118502. https://doi.org/10.1016/j.jclepro.2019.118502.
14. Tan, J.; Lu, W.; Huang, Y.; Wei, S.; Xuan, X.; Liu, L.; Zheng, G. Preliminary study on compatibility of metakaolin-based geopolymer paste with plant fibers. *Constr. Build. Mater.* **2019**, *225*, 772–775. https://doi.org/10.1016/j.conbuildmat.2019.07.142.
15. Zhang, X.; Zhou, X.; Moghaddam, T.B.; Zhang, F.; Otto, F. Synergistic effects of iron (Fe) and biochar on light-weight geopolymers when used in wastewater treatment applications. *J. Clean. Prod.* **2021**, *322*, 129033. https://doi.org/10.1016/j.jclepro.2021.129033.
16. Humberto Tommasini Vieira Ramos, F.J.; Vieira Marques, M.D.F.; de Oliveira Aguiar, V.; Jorge, F.E. Performance of geopolymer foams of blast furnace slag covered with poly(lactic acid) for wastewater treatment. *Ceram. Int.* **2022**, *48*, 732–743. https://doi.org/10.1016/j.ceramint.2021.09.153.
17. Wang, C.; Yang, Z.; Song, W.; Zhong, Y.; Sun, M.; Gan, T.; Bao, B. Quantifying gel properties of industrial waste-based geopolymers and their application in Pb2+ and Cu2+ removal. *J. Clean. Prod.* **2021**, *315*, 128203. https://doi.org/10.1016/j.jclepro.2021.128203.
18. Tchakouté, H.K.; Fotio, D.; Rüscher, C.H.; Kamseu, E.; Djobo, J.N.Y.; Bignozzi, M.C.; Leonelli, C. The effects of synthesized calcium phosphate compounds on the mechanical and microstructural properties of metakaolin-based geopolymer cements. *Constr. Build. Mater.* **2018**, *163*, 776–792. https://doi.org/10.1016/j.conbuildmat.2017.12.162.
19. Yip, C.K.; Lukey, G.C.; van Deventer, J.S.J. The coexistence of geopolymeric gel and calcium silicate hydrate at the early stage of alkaline activation. *Cem. Concr. Res.* **2005**, *35*, 1688–1697. https://doi.org/10.1016/j.cemconres.2004.10.042.
20. Chen, Y.; Shen, C.; Rashid, S.; Li, S.; Ali, B.A.; Liu, J. Biopolymer-induced morphology control of brushite for enhanced defluorination of drinking water. *J. Colloid Interface Sci.* **2017**, *491*, 207–215. https://doi.org/10.1016/j.jcis.2016.12.032.
21. Mirković, M.M.; Pašti, T.D.L.; Došen, A.M.; Čebela, M.Ž.; Rosić, A.A.; Matović, B.Z.; Babić, B.M. Adsorption of malathion on mesoporous monetite obtained by mechanochemical treatment of brushite. *RSC Adv.* **2016**, *6*, 12219–12225. https://doi.org/10.1039/C5RA27554G.
22. Possenti, E.; Colombo, C.; Conti, C.; Gigli, L.; Merlini, M.; Plaisier, J.R.; Realini, M.; Sali, D.; Gatta, G.D. Diammonium hydrogenphosphate for the consolidation of building materials. Investigation of newly-formed calcium phosphates. *Constr. Build. Mater.* **2019**, *195*, 557–563. https://doi.org/10.1016/j.conbuildmat.2018.11.077.
23. Bhattacharyya, K.G.; Gupta, S.S. Removal of Cu(II) by natural and acid-activated clays: An insight of adsorption isotherm, kinetic and thermodynamics. *Desalination* **2011**, *272*, 66–75. https://doi.org/10.1016/j.desal.2011.01.001.
24. Salem, A.; Akbari Sene, R. Removal of lead from solution by combination of natural zeolite–kaolin–bentonite as a new low-cost adsorbent. *Chem. Eng. J.* **2011**, *174*, 619–628. https://doi.org/10.1016/j.cej.2011.09.075.

25. Liu, H.; Peng, S.; Shu, L.; Chen, T.; Bao, T.; Frost, R.L. Magnetic zeolite NaA: Synthesis, characterization based on metakaolin and its application for the removal of Cu2+, Pb2+. *Chemosphere* **2013**, *91*, 1539–1546. https://doi.org/10.1016/j.chemosphere.2012.12.038.
26. Lakherwal, D. Adsorption of heavy metals: A Review. *Int. J. Environ. Res. Dev.* **2014**, *4*, 41–48.
27. Rigaku. *PDXL Integrated X-ray Powder Diffraction Softvare, 2.8.3.0.*; Rigaku: Tokyo, Japan, 2011.
28. International Crystallographical Database (ICDD). **2012**.
29. Barrett, E.P.; Joyner, L.G.; Halenda, P.P. The Determination of Pore Volume and Area Distributions in Porous Substances. I. Computations from Nitrogen Isotherms. *J. Am. Chem. Soc.* **1951**, *73*, 373–380. https://doi.org/10.1021/ja01145a126.
30. Lippens, B.C.; Linsen, B.G.; Boer, J.H.d. Studies on pore systems in catalysts I. The adsorption of nitrogen; apparatus and calculation. *J. Catal.* **1964**, *3*, 32–37. https://doi.org/10.1016/0021-9517(64)90089-2.
31. Zhang, H.; Lu, T.; Zhang, R.; Wang, M.; Krishnan, S.; Liu, S.; Zhou, Y.; Li, D.; Qi, Z. Effects of clay colloids on ciprofloxacin transport in saturated quartz sand porous media under different solution chemistry conditions. *Ecotoxicol. Environ. Saf.* **2020**, *199*, 110754. https://doi.org/10.1016/j.ecoenv.2020.110754.
32. Rüscher, C.H.M.; Elzbieta, M.; Wongpa, J.; Jaturapitakkul, C.; Jirasit, F.; Lohaus, L. Silicate-, aluminosilicate and calciumsilicate gels for building materials: Chemical and mechanical properties during ageing. *Eur. J. Mineral.* **2011**, *23*, 111–124.
33. Sing, K.S.W.; Everett, D.H.; Haul, R.A.W.; Moscou, L.; Pierotti, R.A.; Rouquérol, J.; Siemieniewska, T. Reporting Physisorption Data for Gas/Solid Systems With Special Reference to the Determination of Surface Area and Porosity. *Pure Appl. Chem* **1985**, *57*, 603–619. https://doi.org/10.1351/pac198557040603.
34. Al-Degs, Y.S.; El-Barghouthi, M.I.; El-Sheikh, A.H.; Walker, G.M. Effect of solution pH, ionic strength, and temperature on adsorption behavior of reactive dyes on activated carbon. *Dye Pigment.* **2008**, *77*, 16–23. https://doi.org/10.1016/j.dyepig.2007.03.001.
35. Hamoudi, S.A.; Hamdi, B.; Brendlé, J. Chapter 4.7—Removal of Ions Pb2+ and Cd2+ from Aqueous Solution by Containment Geomaterials. In *Exergetic, Energetic and Environmental Dimensions*; Dincer, I., Colpan, C.O., Kizilkan, O., Eds.; Academic Press: Cambridge, MA, USA, 2018; pp. 1029–1043.
36. Tran, H.N.; You, S.-J.; Hosseini-Bandegharaei, A.; Chao, H.-P. Mistakes and inconsistencies regarding adsorption of contaminants from aqueous solutions: A critical review. *Water Res.* **2017**, *120*, 88–116. https://doi.org/10.1016/j.watres.2017.04.014.
37. Lazaridis, N.K.; Asouhidou, D.D. Kinetics of sorptive removal of chromium(VI) from aqueous solutions by calcined Mg–Al–CO3 hydrotalcite. *Water Res.* **2003**, *37*, 2875–2882. https://doi.org/10.1016/S0043-1354(03)00119-2.
38. Nethaji, S.; Sivasamy, A.; Mandal, A.B. Adsorption isotherms, kinetics and mechanism for the adsorption of cationic and anionic dyes onto carbonaceous particles prepared from Juglans regia shell biomass. *Int. J. Environ. Sci. Technol.* **2013**, *10*, 231–242. https://doi.org/10.1007/s13762-012-0112-0.
39. Langmuir, I. The adsorption of gases on plane surfaces of glass, mica and platinum. *J. Am. Chem. Soc.* **1918**, *40*, 1361–1403. https://doi.org/10.1021/ja02242a004.
40. Yavari, S.; Mohammad, M.N.; Teymouri, P.; Shahmoradi, B.; Maleki, A. Cobalt ferrite nanoparticles: Preparation, characterization and anionic dye removal capability. *J. Taiwan Inst. Chem. Eng.* **2016**, *59*, 320–329. https://doi.org/10.1016/j.jtice.2015.08.011.
41. de Sá, A.; Abreu, A.S.; Moura, I.; Machado, A.V. 8—Polymeric materials for metal sorption from hydric resources. In *Water Purification*; Grumezescu, A.M., Ed.; Academic Press: Cambridge, MA, USA, 2017; pp. 289–322.
42. Davod Ghahremani, I.M.S.A.M. Sorption thermodynamic and kinetic studies of Lead removal from aqueous solutions by nano Tricalcium phosphate. *Bull. De La Société R. Des Sci. De Liège [En Ligne]* **2017**, *86*, 96–112.
43. Safatian, F.; Doago, Z.; Torabbeigi, M.; Rahmani Shams, H.; Ahadi, N. Lead ion removal from water by hydroxyapatite nanostructures synthesized from egg sells with microwave irradiation. *Appl. Water Sci.* **2019**, *9*, 108. https://doi.org/10.1007/s13201-019-0979-8.
44. Lan, T.; Guo, S.; Li, X.; Guo, J.; Bai, T.; Zhao, Q.; Yang, W.; Li, P. Mixed precursor geopolymer synthesis for removal of Pb(II) and Cd(II). *Mater. Lett.* **2020**, *274*, 127977. https://doi.org/10.1016/j.matlet.2020.127977.